Published OnlineFirst September 11, 2015; DOI: 10.1158/0008-5472.CAN-14-3636

Microenvironment and Immunology

Cancer Research

Elevated Expression of the C-Type Lectin CD93 in the Glioblastoma Vasculature Regulates Cytoskeletal Rearrangements That Enhance Vessel Function and Reduce Host Survival

Elise Langenkamp[1], Lei Zhang[1], Roberta Lugano[1], Hua Huang[1], Tamador Elsir Abu Elhassan[2], Maria Georganaki[1], Wesam Bazzar[1], Johan Lööf[1], George Trendelenburg[3], Magnus Essand[1], Fredrik Pontén[1], Anja Smits[2,4], and Anna Dimberg[1]

Abstract

Glioblastoma is an aggressive brain tumor characterized by an abnormal blood vasculature that is hyperpermeable. Here, we report a novel role for CD93 in regulating angiogenesis in this setting by modulating cell–cell and cell–matrix adhesion of endothelial cells. Tissue microarray analysis demonstrated that vascular expression of CD93 was correlated with poor survival in a clinical cohort of patients with high-grade astrocytic glioma. Similarly, intracranial growth in the GL261 mouse model of glioma was delayed significantly in CD93$^{-/-}$ hosts, resulting in improved survival compared with wild-type mice. This effect was associated with increased vascular permeability and decreased vascular perfusion of tumors, indicating reduced vessel functionality in the absence of CD93. RNAi-mediated attenuation of CD93 in endothelial cells diminished VEGF-induced tube formation in a three-dimensional collagen gel. CD93 was required for efficient endothelial cell migration and proper cell polarization *in vitro*. Further, in endothelial cells where CD93 was attenuated, decreased cell spreading led to a severe reduction in cell adhesion, a lack of proper cell contacts, a loss of VE-cadherin, and aberrant actin stress fiber formation. Our results identify CD93 as a key regulator of glioma angiogenesis and vascular function, acting via cytoskeletal rearrangements required for cell–cell and cell–matrix adhesion. *Cancer Res; 75(21); 4504–16. ©2015 AACR.*

Introduction

Glioblastomas are highly malignant brain tumors that are characterized by nuclear atypia, high proliferative index, necrosis, endothelial proliferation and pleomorphic, abnormal vessels (1, 2). The tumor vessels are malfunctioning and hyperpermeable, aggravating the condition by giving rise to brain edema (3). Therefore, combining conventional cancer therapy with specific targeting of the abnormal tumor vessels represents an attractive approach for treatment of patients with glioma. Antiangiogenic therapy neutralizing VEGF or its receptor VEGFR2 improves survival in animal models of glioma and is in clinical use as a second-line treatment for glioblastoma (4, 5). Still, therapies targeting the VEGF/VEGFR2 pathway have not resulted in prolongation of overall survival of patients with glioblastoma, despite a significant improvement in progression-free survival. Resistance mechanisms leading to upregulation of other proangiogenic factors or toxicities arising due to the important role of VEGF/VEGFR2 signaling in normal physiology may contribute to these disappointing results. An alternative strategy is to exploit the heterogeneity of gene expression in tumor endothelial cells as compared with normal endothelial cells, and target molecules specifically expressed in the tumor vasculature that contribute to angiogenesis and vascular malformation in glioblastoma (6–9).

Through laser capture microdissection followed by microarray analysis of gene expression, we have recently characterized the transcriptome of blood vessels in human glioblastoma, low-grade glioma, and control brain tissue. We identified 95 genes that are specifically expressed in glioblastoma vasculature, including the single-pass transmembrane glycoprotein CD93 (7). CD93 consists of an extracellular part with a C-type lectin-like domain (CTLD), five tandem EGF-like repeats, a serine-threonine–rich mucin-like domain, a transmembrane domain, and a short cytoplasmic domain (10). It is prominently expressed in endothelial cells and some hematopoietic subsets, and can be shed and released in a soluble form (sCD93) upon inflammatory stimuli (11, 12). CD93$^{-/-}$ mice have no reported vascular defects and are born at normal mendelian ratios, but show defects in clearance of apoptotic cells and a slightly decreased maintenance of antibody secretion (13, 14).

[1]Department of Immunology, Genetics and Pathology, Science for Life Laboratory, The Rudbeck Laboratory, Uppsala University, Uppsala, Sweden. [2]Department of Neuroscience, Neurology, University Hospital Uppsala, Uppsala, Sweden. [3]Department of Neurology, University Medicine Goettingen, Göttingen, Germany. [4]Department of Neurology, Danish Epilepsy Center, Dianalund, Denmark.

Note: Supplementary data for this article are available at Cancer Research Online (http://cancerres.aacrjournals.org/).

L. Zhang and R. Lugano contributed equally to this article.

Corresponding Author: Anna Dimberg, Department of Immunology, Genetics and Pathology, Rudbeck Laboratory, Uppsala University, SE-75185 Uppsala, Sweden. Phone: 46-70-166496; Fax: 46-18-6110222; E-mail: Anna.Dimberg@igp.uu.se

doi: 10.1158/0008-5472.CAN-14-3636

Published OnlineFirst September 11, 2015; DOI: 10.1158/0008-5472.CAN-14-3636

A recent study has identified CD93 as one of the top 20 genes of a core human primary tumor angiogenesis signature highly expressed in head and neck squamous cell carcinomas, breast cancers, and clear cell renal cell carcinomas (15). Consistent with a role for CD93 in angiogenesis, a recombinant protein containing the EGF-like domain and the serine-threonine–rich mucin-like domain of CD93 has been demonstrated to have proangiogenic properties, but the effects were moderate and less evident in total sCD93 where the CTLD is included (16). Moreover, an antibody recognizing the extracellular domain of CD93 is able to inhibit proliferation, migration, and sprouting of human endothelial cells (17). Although the main site of CD93 expression is the vascular endothelium, apart from the above-mentioned studies, its role in vascular biology and function has not been investigated.

To understand the role of CD93 in glioblastoma vessels and its effect on tumor growth, we investigated CD93 function in tumor angiogenesis and endothelial cell biology. Interestingly, we observed prolonged survival of $CD93^{-/-}$ mice bearing orthotopic GL261 gliomas as compared with wild-type mice, associated with decreased tumor vessel perfusion and enhanced leakage in $CD93^{-/-}$ mice. Consistent with a role of CD93 in orchestrating angiogenesis, we found that knockdown of CD93 inhibits tube formation, adhesion, and migration of endothelial cells *in vitro* due to defects in cytoskeletal rearrangement and loss of endothelial adherence junctions. Importantly, high CD93 expression in tumor vessels was significantly correlated with shorter survival in a clinical cohort of patients with grade III–IV astrocytic gliomas. Together, our data imply that CD93 is a key regulator of glioma angiogenesis and vascular function through the control of cell–cell and cell–matrix adhesion.

Materials and Methods

Tissue microarray and image analysis

Vascular expression of CD93 was analyzed in tissue microarrays containing duplicate tissue cores per sample (1 mm diameter) of 235 biopsies of human low-grade (WHO grade II) and high-grade (WHO grades III and IV) gliomas of various histologic subtypes, and nonmalignant brain tissue (gliosis and normal gray and white matter) used as controls (Supplementary Table S1). Human tissue was obtained in a manner compliant with the Declaration of Helsinki. The Ethics Review Board in Uppsala approved the use of human samples and participation of patients occurred after informed consent.

Immunohistochemical staining was performed as described (18) using a rabbit antibody to CD93 (HPA009300; Atlas Antibodies) and 3'3'-diaminobenzidine as substrate. The frequency of positively stained vessels was scored in a blinded fashion on a scale from 0 to 2 (0 = no vessels stained, 1 = minority of vessels stained, 2 = majority of vessels stained).

Tumor cell and primary endothelial cell and pericytes culture

T241 fibrosarcoma, B16.F10 melanoma (American Type Culture Collection via LGC Standards), and GL261 glioma cells (kind gift from Dr. Geza Safrany, NRIRR) engineered to express luciferase in house (L. Zhang and A. Dimberg; unpublished data) were cultured on 10-cm culture dishes in DMEM (Life Technologies) supplemented with 10% FCS (Sigma-Aldrich) at 37°C and 5% CO_2/95% air in a humidified chamber.

Human Dermal Microvascular Endothelial Cells (HDMEC; 3H Biomedical; PromoCell) were cultured up to passage 15 on gelatin-coated culture dishes in Endothelial Cell Basal Medium with full supplements (EBM-MV2; PromoCell) at 37°C and 5% CO_2/95% air in a humidified chamber. Human Brain Pericytes (HBP; 3H Biomedical) were cultured on culture dishes in Pericyte Medium (PM; 3H Biomedical) at 37°C and 5% CO_2/95% air in a humidified chamber. Cell lines were not authenticated after purchase (B16, T241) or after transfer from other laboratories (GL261) but were routinely tested negative for mycoplasma using the Mycoplasma Detection Kit (Lonza).

Mice

$CD93^{-/-}$ C57Bl/6 mice (13) were bred in house. C57Bl/6 wild-type mice were purchased from Taconic M&B. All animal work was performed according to the guidelines for animal experimentation and welfare provided by Uppsala University and approved by the Uppsala County regional ethics committee.

Tumor studies

GL261 glioma cells expressing luciferase were orthotopically injected in the brain of $CD93^{-/-}$ and wild-type C57Bl/6 mice, and tumor development was monitored by bioluminescence imaging as described in Supplementary Materials and Methods.

For the survival study, mice were sacrificed by cervical dislocation when they showed more than 10% weight loss, and brains were excised, snap-frozen on isopentane/dry ice, and stored at −80°C for further analysis.

To study vascular perfusion, mice were injected with 100 μL of 1 mg/mL FITC-labeled or biotin-labeled lycopersicon esculentum lectin (Vector Laboratories) in the tail vein or the orbital plexus at days 21 to 24. The lectin was allowed to circulate for 10 to 30 minutes, after which the mice were perfused with PBS followed by 4% PFA through the heart under isoflurane or ketamine/xylazine anesthesia. The brains were excised, fixed in 4% PFA for 2 hours, and either dehydrated in 30% sucrose/PBS overnight, embedded in OCT Cryomount (Histolabs), and snap-frozen on isopentane/dry ice for cryosectioning, or directly used for sectioning on a vibratome.

$CD93^{-/-}$ and wild-type C57Bl/6 mice were subcutaneously injected in the right flank with 100,000 B16.F10 or 500,000 T241 cells in 100 μL phosphate-buffered saline under anesthesia by inhalation of isoflurane/O_2. Tumors were measured by calipers, and the volume was calculated according to the formula: tumor volume = $0.52 \times \text{length} \times \text{width}^2$. At day 15 (B16.F10) or day 20 (T241), mice were sacrificed by cervical dislocation and tumors were excised. The wet weight was determined and tumors were snap-frozen on isopentane/dry ice and stored at −80°C.

siRNA transfections

HDMEC were incubated with scrambled control siRNA or siRNA to CD93 (Hs_CD93_1 and Hs_C1QR1_5; FlexiTube; Qiagen) at a concentration of 2 nmol/L in a mixture of 20% OptiMem (Life Technologies) in endothelial cell medium supplemented with 30 μL/mL RNAiMAX lipofectamine (Life Technologies) for 4 to 6 hours, after which the medium was replaced with fresh medium. Experiments were performed at days 2 to 3 after siRNA transfection.

Lentivirus construction, production, and HDMEC infection

cDNA sequences for human CD93 (WT-CD93) and CD93 with a 5 amino acid (606–610) deletion (CD93-Cyto5Aa, reported

Published OnlineFirst September 11, 2015; DOI: 10.1158/0008-5472.CAN-14-3636

CD93-Cyto5Aa, lacking the reported moesin binding site) were designed, and mutant HDMEC were obtained as described in Supplementary Material and Methods.

Tube formation assay

siRNA-transfected HDMEC were seeded onto a three-dimensional (3D) collagen-1 gel and stimulated with 50 ng/mL VEGF for 24 hours as described (19). The resulting tubes were fixed in ZincFix, stained with Texas Red–labeled phalloidin (Life Technologies), and analyzed by confocal microscopy. The total phalloidin-positive tube area was quantified using ImageJ and normalized to the number of Hoechst-positive nuclei.

dsRed-transfected HDMEC were transfected with scrambled siRNA and mixed in a tube formation assay with unlabeled cells that were transfected with siRNA to CD93, and vice versa. Tubes were visualized by staining with Alexa Fluor 647–labeled phalloidin and analyzed by confocal microscopy. The ability of HDMEC to form luminized tube-like structures was assessed as previously described (20). See Supplementary Materials and Methods.

Proliferation and apoptosis

Proliferation of siRNA-transfected HDMEC cultured in EBM and HBP cultured in conditioned media derived from siRNA-transfected HDMEC was assessed by cell counting during a time period of 4 days. Apoptosis in siRNA-transfected HDMEC was assessed by detection of cleaved caspase-3 activity using a colorimetric assay as described in Supplementary Material and Methods.

Migration assay

Confluent siRNA-transfected HDMEC were serum starved in EBM with 1% FCS. Scrape wounds were produced on the cell monolayer, and wound repair was analyzed under ×150 magnification (PlanApo S 1.0x objective) up to 8 hours, using a stereomicroscope (SteREO Discovery.V12; Zeiss) attached to a digital camera (AxioCam; Zeiss). Alternatively, at 4 hours after wounding, the cells were fixed for immunolabeling and confocal microscopy analysis as described in Supplementary Materials and Methods.

Adhesion assay

siRNA-transfected HDMEC were seeded out in EBM supplemented with 0.2% BSA at 10,000 cells per well in a gelatin-coated 96-well plate. After 30 minutes, the wells were washed with PBS to remove nonadherent cells, and the number of adhering cells was quantified using the CyQUANT-GR cell quantification Kit (Life Technologies). Fluorescence with an excitation at 480 nm and emission at 520 nm was measured using a Wallac Victor fluorescence plate reader. Alternatively, at 30 minutes after seeding, cells were fixed with 4% PFA for immunolabeling and confocal microscopy.

Western blot and coimmunoprecipitation

Protein level of CD93 and moesin was assessed by Western blot, and coimmunoprecipitation for CD93 was performed with the Pierce co-immunoprecipitation Kit (Thermo Scientific) as described in Supplementary Materials and Methods.

RNA extraction and qPCR

RNA from siRNA-treated endothelial cells *in vitro* was extracted using the RNeasy Plus Mini Kit (Qiagen). Total RNA was transcribed using Superscript III reverse transcriptase in a 20-μL total volume containing 250 ng of random hexamers and 40 units of RNAse OUT inhibitor (all from Life Technologies). mRNA expression of CD93 was quantified relative to the house keeping gene HPRT by real-time PCR in duplicate reactions per sample with 0.25 μmol/L forward and reverse primer in SYBR Green PCR Master Mix (Life Technologies).

Immunofluorescent staining of HDMEC

siRNA-transfected HDMEC were immunofluorescently stained for Golgin-97 to visualize the Golgi complex and for VE-Cadherin to visualize the cell–cell junctions as described in Supplementary Materials and Methods.

Immunofluorescent and immunohistochemical staining of tumor sections

Cryosections and vibratome sections from GL261 gliomas and T241 fibrosarcomas were immunofluorescently stained for CD31, CD45, CD93, podocalyxin, cleaved caspase-3, GLUT-1, and Collagen IV and immunohistochemically stained for CD93 as described in Supplementary Materials and Methods.

Statistical analysis

Statistical significance of the observed differences was addressed by statistical tests using GraphPad Prism V6.01 (GraphPad Software).

Survival curves were plotted according to the Kaplan–Meier method (product-limit method), and the log-rank probability test (Mantel–Cox) estimated the prognostic value of the CD93 expression in the univariate analysis. The Cox proportional hazard model was used to calculate the impact of CD93 expression in the multivariate analysis of high-grade gliomas together with established prognostic factors (malignancy grade, patient age, extent of tumor resection, and postoperative therapy). The level for confounders to be removed from the model when adjusted for variables already in the model (p-to-remove) was set to >0.1. Natural logarithm (ln) cumulative hazard plots were made to confirm the assumption of the proportional hazard functions. The significant prognostic factors in the stepwise model were also analyzed as products to minimize the possibility of interaction. JMP, version 10.0 (SAS Institute Inc.) was used for statistical analysis.

Results

Vascular expression of CD93 correlates to tumor grade in human glioma

We previously demonstrated that high vascular density, vascular abnormalization, and formation of glomeruloid microvascular proliferations are characteristic features of grade IV glioma, and that these aberrant vessels produce high levels of CD93 mRNA and protein (7). In order to extend our analysis of CD93 protein expression in tumor vessels in a larger material, we scored the fraction of blood vessels staining positive for CD93 in several tumor tissue microarrays that contained a total of 235 biopsies of human control brain and grade II, grade III, and grade IV glioma tissues of various histologic subtypes. This demonstrated that in 73% of the grade IV glioma samples, the majority of the blood vessels stained positive for CD93 (Fig. 1A and B). The fraction of CD93-positive vessels was significantly lower in respectively grade III and grade II glioma, and even further reduced in control brain samples, where 33% did not display any CD93 staining in the vasculature at all. Staining of larger sections of human

Published OnlineFirst September 11, 2015; DOI: 10.1158/0008-5472.CAN-14-3636

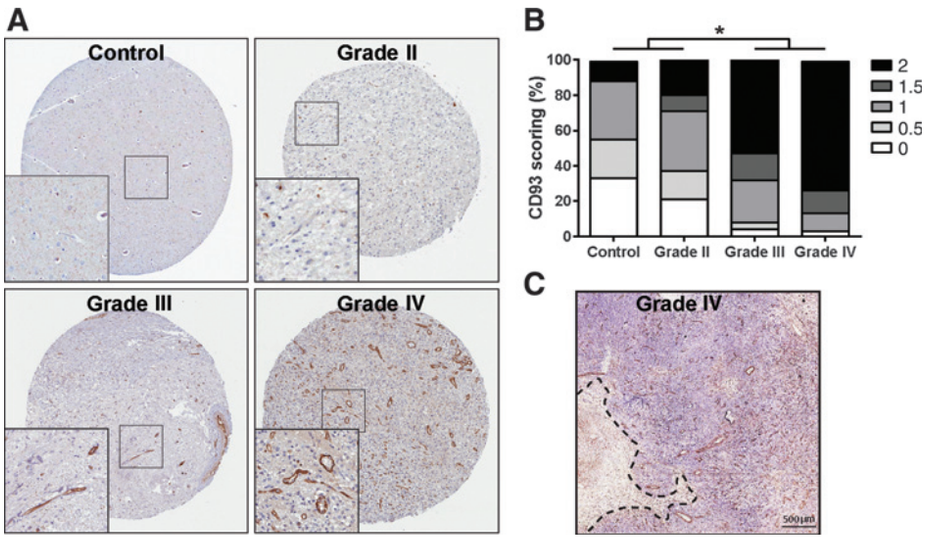

Figure 1.
CD93 expression was increased in high-grade human glioma vasculature. Immunohistochemical staining of CD93 expression (A) and semiquantitative scoring of the fraction of positive blood vessels (B) in human glioma tissue microarrays. In a total of 235 human glioma and nonmalignant control brain biopsies, the frequency of positively staining vessels was scored on a scale from 0 to 2 (0, no vessels stained; 1, minority of vessels stained; 2, majority of vessels stained). Results were averaged and plotted as percentage of samples per score in nonmalignant control brain (9 biopsies), grade II (82 biopsies), grade III (54 biopsies), and grade IV samples (90 biopsies; *, $P < 0.0001$; Kruskal–Wallis test with Dunne posttest). C, CD93 distribution in grade IV glioma vasculature. The lower magnification image shows no gross difference in CD93 distribution within the tumor area. Dotted line represents the migrating front of tumor cells.

glioblastoma tissue revealed that CD93-positive vessels were present both within the core and the invading front of the tumor (Fig. 1C). As demonstrated in Supplementary Table S1, the fraction of CD93-positive vessels was slightly higher in ependymoma compared with oligoastrocytoma and oligodendroglioma, whereas the largest CD93 positivity was found in gliosarcoma and glioblastoma.

CD93 deficiency impairs GL261 glioma and T241 fibrosarcoma growth in female mice

To investigate the role of CD93 in glioma growth, we employed the murine GL261 glioma model implanted orthotopically in the mouse brain. We first checked the expression pattern of CD93 in GL261 glioma by immunohistochemical and immunofluorescent staining. This revealed that CD93 was mainly expressed in the vasculature of the GL261 glioma, and that CD93 staining was more intense in the tumor vessels than in the vasculature of the surrounding brain (Fig. 2A). Moreover, the GL261 glioma vessels displayed an abnormal phenotype of malformed vessels, similar to that found in human glioblastoma (Fig. 1A). Immunofluorescent costaining with CD31 and CD45 demonstrated that CD93 was highly expressed by the vasculature and not detected in infiltrating leukocytes or GL261 tumor cells (Fig. 2B and C). No CD93 staining was detected in GL261 tumors in $CD93^{-/-}$ mice (Fig. 2D–F).

We implanted GL261 cells expressing luciferase stereotactically in the brains of female CD93-deficient and wild-type mice, and performed bioluminescence imaging to measure tumor volume at different days after tumor cell inoculation. Although the glioma growth curves appeared to have a similar slope, the brain tumors of $CD93^{-/-}$ mice reached a measurable size (>100,000 bioluminescence units) on average 11 days later than the brain tumors of wild-type mice (Fig. 2G and H). This was associated with a significantly longer survival after tumor cell injection in CD93-deficient mice compared with wild-type mice (Fig. 2I).

To analyze whether CD93 deficiency affects growth of other tumor types as well, we employed the subcutaneously growing T241 fibrosarcoma and B16.F10 melanoma models. We found that T241 growth was significantly reduced in female CD93-deficient mice compared with wild-type mice (Fig. 2J). This was confirmed by the differences in weight of the tumors taken at day 20 after tumor cell injections (Fig. 2K). In contrast, B16 melanoma tumors grew equally well in $CD93^{-/-}$ and wild-type mice (Supplementary Fig. S1A and S1B). Interestingly, in male $CD93^{-/-}$ mice, we did not detect any difference in tumor growth in either the GL261 or the T241 tumor model (Supplementary Fig. S1C–S1E).

Knockdown of CD93 inhibits formation of tube-like structures *in vitro*

To investigate the role of CD93 in endothelial cell biology, we used RNA interference to knock down its expression in HDMEC *in vitro*. Transfection of HDMEC with siRNA to CD93 reduced its mRNA expression by 95% to 99%, which resulted in an efficient downregulation of CD93 protein that persisted for at least 3 days (Fig. 3A).

We first investigated if CD93 has a role in endothelial cell proliferation or survival, and found that siRNA-mediated knockdown of CD93 did not affect the proliferation rate or apoptosis of HDMEC (Supplementary Fig. S2A and S2B). Because we previously showed that CD93 mRNA is upregulated when HDMEC form tube-like structures on a 3D collagen gel in response to VEGF (7), we next investigated how siRNA-mediated knockdown of CD93 affects the formation of these tubes. While

Published OnlineFirst September 11, 2015; DOI: 10.1158/0008-5472.CAN-14-3636

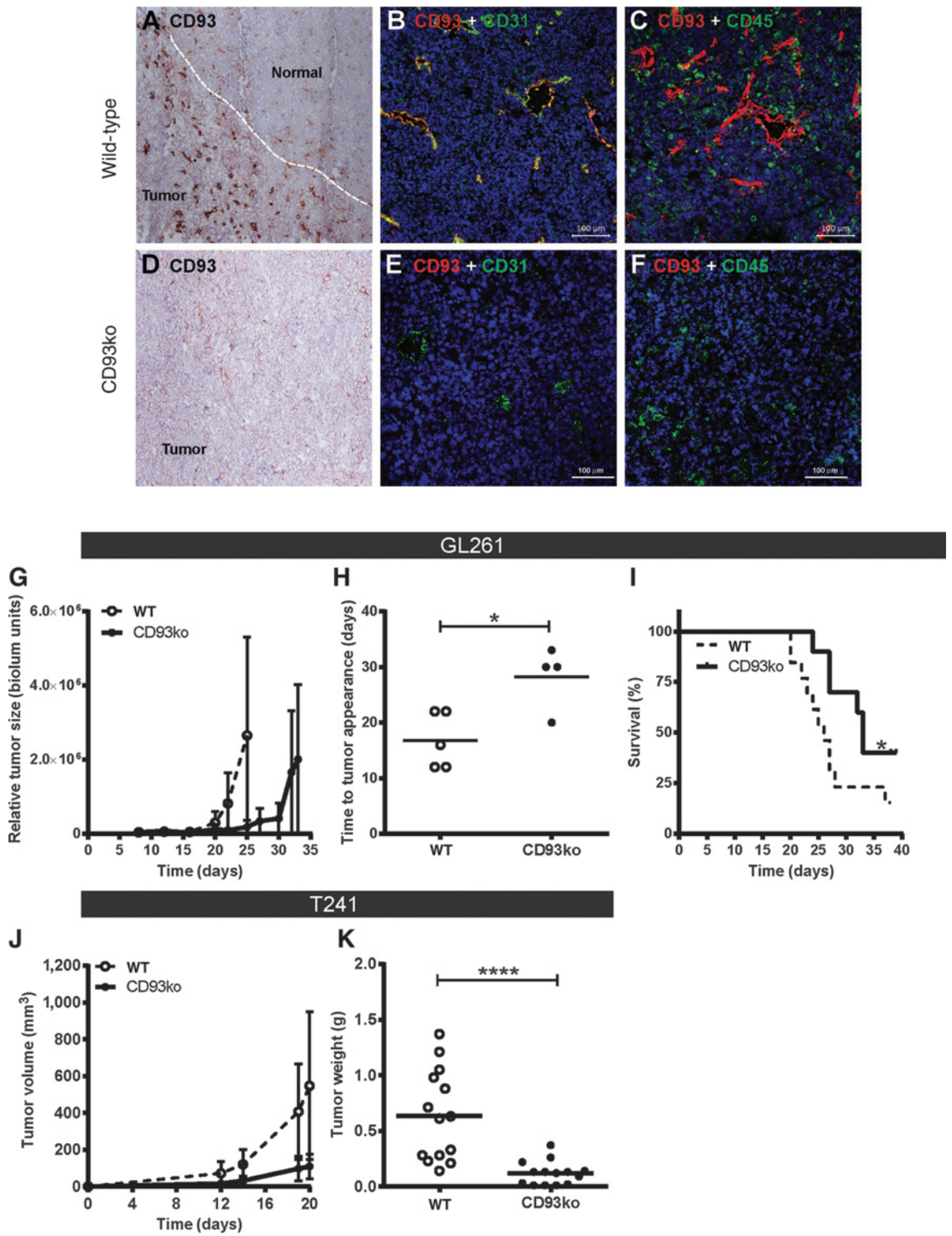

Figure 2.
CD93 deficiency delayed GL261 glioma outgrowth in female mice. A–C, CD93 is prominently expressed in the abnormal blood vessels of GL261 glioma, yet less intense in the vasculature of the surrounding brain (A; immunohistochemical staining of CD93), and not in the tumor-infiltrating leukocytes (B and C; immunofluorescent costaining of CD93 with CD31 and CD45). D–F, validation of CD93 antibody specificity in GL261 glioma grown in $CD93^{-/-}$ mice. Immunohistochemical staining of CD93 (D). Immunofluorescent costaining of CD93 with CD31 and CD45 in $CD93^{-/-}$ mice (E–F). G–I, GL261 growth in $CD93^{-/-}$ and wild-type (wt) female C57Bl/6 mice. G, bioluminescence-based quantification of tumor size (mean ± SD, $n = 7$ for wild-type and $n = 5$ for CD93ko; this includes two wild-type mice and one $CD93^{-/-}$ mouse without tumor take). H, values depict the number of days after which the tumor reached a luminescence intensity >100,000 units and became visible in the IVIS imager, calculated from the day of injection. (*Continued on the following page.*)

Published OnlineFirst September 11, 2015; DOI: 10.1158/0008-5472.CAN-14-3636

control-transfected cells formed a network of tube-like structures in the collagen gel after 24 hours of stimulation with VEGF, cells that were transfected with siRNA to CD93 lost the capacity to form contacts with neighboring cells and establish tubes (Fig. 3C–F). Quantification of the total area of the tubular network, normalized to cell number, revealed that CD93 knockdown significantly impaired tube formation by HDMEC (Fig. 3B).

Because the efficiency of tubular network formation is also influenced by the density of the cells, we accounted for differences in cell number by mixing control-transfected dsRed-labeled HDMEC on a 1:1 and a 1:2 ratio with unlabeled HDMEC that were transfected with siRNA to CD93. Phalloidin labeling to visualize the unlabeled cells (Fig. 3G; depicted in green) revealed that only the dsRed-labeled control cells were able to participate in the network of tube-forming cells, whereas unlabeled cells in which CD93 expression was knocked down did not take part in formation of these structures. When the reverse experiment was performed, only the unlabeled HDMEC with normal levels of CD93 took part in the formation of tube-like structures (Fig. 3H). Through dispersion of endothelial cells within a collagen gel, we found that although endothelial cells failed to make long tubular networks after CD93 knockdown, the short tube-like structures that formed contained lumens (Fig. 3I–P). This suggests that CD93 contributes to angiogenesis by promoting tubular morphogenesis, but that CD93 is dispensable for lumen formation.

Knockdown of CD93 inhibits endothelial cell adhesion and migration *in vitro*

The process of tubular morphogenesis requires cells to adhere to the extracellular matrix, migrate, and to establish cell–cell contacts with one another. To investigate which of these aspects are controlled by CD93, we first studied whether CD93 knockdown affects the migratory capacity of HDMEC in a scratch assay. Although control-transfected HDMEC had covered around 80% of the wound area at 8 hours after the scratch, HDMEC transfected with CD93 siRNA had covered only around 56% of the wound area, showing that CD93 knockdown inhibits HDMEC migration (Fig. 4A and B). To determine if the inhibition of migration upon CD93 knockdown was related to defects in cytoskeletal rearrangement, we stained the migrating front in control and CD93 siRNA-treated cells with an antibody recognizing golgin-97 to visualize the Golgi. The orientation of the Golgi in relation to the direction of migration was analyzed as a marker of correct cell polarization (Supplementary Fig. S2C and S2D; ref. 21). We found that in mock-transfected and control siRNA-transfected cells, the majority of endothelial cells were correctly polarized, whereas CD93 knockdown resulted in a significant increase in the number of nonpolarized cells and a disorganized leading edge of the migrating front (Fig. 4C–G).

We then tested whether CD93 knockdown affects endothelial cells adhesion to a gelatin-coated surface. Immunofluorescent staining of cells 30 minutes after seeding revealed that knockdown of CD93 resulted in markedly diminished spreading of endothelial cells (Fig. 4H–K). Consistent with this, CD93 knockdown significantly reduced the number of adherent cells (Fig. 4L). As the intracellular domain of CD93 has been demonstrated to bind to moesin, a member of the ezrin/radixin/moesin (ERM) family of proteins that interact with cytoskeletal actin (22), we investigated how knockdown of CD93 affects the organization of the cytoskeleton by immunofluorescently labeling cells with phalloidin. While the control cells formed a regular monolayer, the cells in which CD93 was knocked down displayed strong stress fiber formation and formed only limited contacts with one another (Fig. 5A–H). Immunofluorescent staining of VE-cadherin confirmed striking defects in adherens junction formation after CD93 knockdown (Fig. 5I–P). The formation of interendothelial junctions was restored by lentiviral transfection with a wild-type CD93 construct, but not by transfection with a mutant CD93 construct lacking the reported moesin-binding site (Cyto 5Aa CD93). This is consistent with a role for CD93 in controlling cytoskeletal organization at least partially through interaction with moesin (Supplementary Fig. S2E–S2S).

Perfusion of glioma vasculature is reduced in CD93-deficient mice

To determine what underlies the decreased tumor growth in $CD93^{-/-}$ mice, we analyzed necrosis, hypoxia, and apoptosis of tumor cells in T241 and GL261 tumors. Decreased necrosis was found in GL261 tumors, but not in T241 tumors, in $CD93^{-/-}$ mice compared with wild-type mice, which correlated to the smaller tumor size (Supplementary Fig. S3A–S3H). We noted a trend toward increased hypoxia, as assessed by GLUT-1 staining, in both T241 and GL261 tumors while enhanced apoptosis was found only in T241 tumors in $CD93^{-/-}$ mice (Supplementary Fig. S3I–S3T).

Because our data suggest a role for CD93 in tubulomorphogenesis, we investigated whether CD93 deficiency affected tumor angiogenesis in GL261 tumors. Enlarged vessels with an abnormal morphology were found in GL261 tumors of both wild-type and $CD93^{-/-}$ mice, and no differences in vessel density or vascular morphology were noted by stereological analysis of vessel area and diameter in GL261 glioma (Fig. 6A–C; Supplementary Fig. S4B and S4C), nor in T241 fibrosarcoma (Supplementary Fig. S4A). Similarly, T241 and GL261 tumor vessels in $CD93^{-/-}$ and wild-type mice were equally covered by desmin-positive pericyte (Supplementary Fig. S4H-M). Consistent with this, endothelial-derived soluble CD93 did not affect *in vitro* pericyte proliferation (Supplementary Fig. S4F–S4G).

Because CD93 knockdown affected endothelial polarization with respect to the direction of migration (Fig. 4C–G), we analyzed polarization of tumor vessels by staining for podycalyxin (luminal marker) in combination with collagen IV (basement membrane). We found that while vessels in T241 tumors were correctly polarized in both $CD93^{-/-}$ and wild-type mice, GL261 tumor vessels were structurally abnormal and the polarization was at least partially disrupted in both genotypes (Supplementary Fig. S5A–S5O). Interestingly, through staining for endogenous IgG, we found a striking increase in vascular permeability in GL261 tumors from $CD93^{-/-}$ mice (Fig. 6D–F).

(*Continued.*) Each value corresponds to one mouse (*, $P < 0.05$, Mann–Whitney *U* test). I, Kaplan–Meier survival curve of mice injected with GL261 glioma cells; mice were sacrificed when they suffered from more than 15% loss of body weight, relative to the body weight at the start of the experiment (*, $P < 0.05$, $n = 10$–13, Gehan–Breslow–Wilcoxon test). J and K, tumor volumes (J; mean ± SD, $n = 15$) and endpoint weight (K; mean) of T241 fibrosarcoma growing subcutaneously in the right flank of female $CD93^{-/-}$ and wild-type mice. Tumor sizes were measured by calipers every 2 to 3 days, and tumor weights were determined at day 20 (****, $P < 0.0001$, Mann–Whitney *U* test).

Published OnlineFirst September 11, 2015; DOI: 10.1158/0008-5472.CAN-14-3636

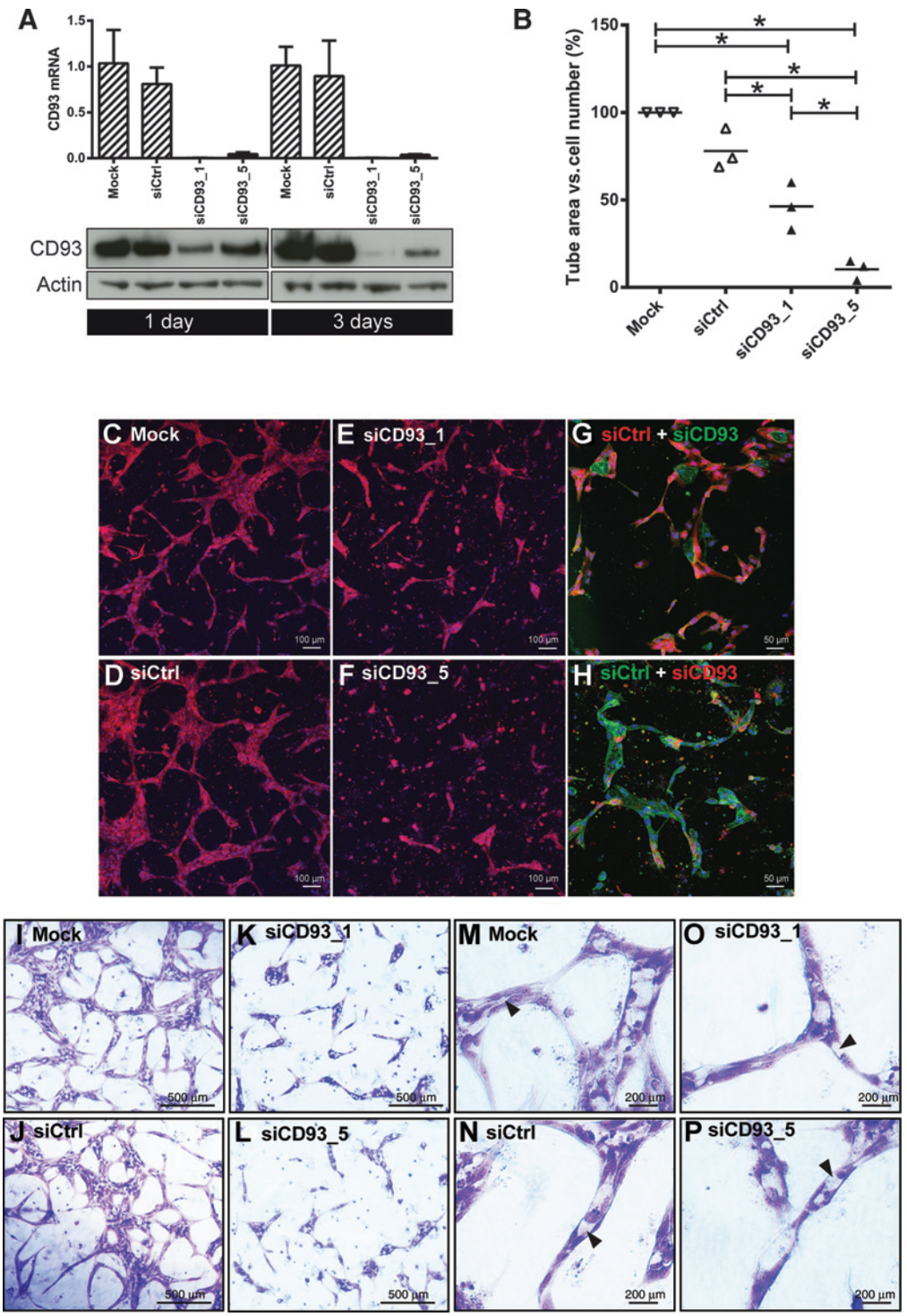

Figure 3.
CD93 knockdown impaired tube formation of HDMEC. A, the expression of CD93 in HDMEC was efficiently inhibited by RNA interference. Values depict fold change in CD93 mRNA expression relative to HPRT as a housekeeping gene (mean + SD), and bands depict CD93 protein and actin as a housekeeping gene at 1 and 3 days after siRNA transfection. B–F, HDMEC transfected with siRNA to CD93 and control-transfected cells were allowed to form tube-like structures on a 3D collagen gel under VEGF stimulation for 24 hours, fixed, and stained with phalloidin. Total tubular area was quantified and adjusted to the number of Hoechst-positive nuclei to account for differences in cell number (B; each value depicts the mean of 3 to 4 wells in a separate experiment; *, $P < 0.05$, one-way ANOVA with Bonferroni correction for multiple comparisons). G and H, in a separate experiment, dsRed-labeled HDMEC were transfected with control siRNA and mixed in a tube formation assay with unlabeled cells that were transfected with siRNA to CD93. (*Continued on the following page.*)

Published OnlineFirst September 11, 2015; DOI: 10.1158/0008-5472.CAN-14-3636

Perfusion of glioma-bearing mice with lycopersicon esculentum (tomato) lectin revealed that the percentage of vessels that were perfused was significantly reduced in CD93$^{-/-}$ male and female mice (Fig. 6G and H). Important to note is that even vessels that showed only small traces of lectin-positivity (Fig. 6L–N) were considered as perfused in the quantification. These vessels constituted the majority of perfused blood vessels in CD93$^{-/-}$ mice and created a strong contrast with the well-perfused vessels in wild-type mice that showed the presence of FITC-lectin along the whole vascular lining (Fig. 6I–K). These data demonstrate that CD93 promotes formation of functional vasculature in mouse glioma.

Tumor vascular expression of CD93 is indicative of poor survival for patients with high-grade astrocytic gliomas

Due to the difference in glioma growth and tumor vascular perfusion between CD93$^{-/-}$ and wild-type mice and the striking effects of CD93 knockdown on the endothelial cytoskeletal rearrangement, we analyzed if expression of CD93 in tumor vessels correlated to survival. For this analysis, we included the high-grade astrocytic tumors that were part of a previously described clinical cohort (23). High-grade ependymomas, gliosarcomas, and anaplastic oligodendrogliomas were excluded from this analysis. Patients were dichotomized into high or low vascular CD93-expressing groups according to the averages of the CD93 staining in the glioma tissue microarrays (Fig. 1; Supplementary Table S1). The Kaplan–Meier survival curve revealed that patients with clear CD93 expression in the majority of their tumor vasculature (CD93 score $\geq$ 1.5) had a significantly shorter survival than patients that expressed CD93 in the minority of vessels (CD93 score $\leq$ 1.0; Fig. 7, $P = 0.0417$, log-rank test). CD93 expression was identified as an independent predictor of survival in the multivariate analysis ($P = 0.0479$, Cox proportional hazard), together with established clinical prognostic factors for these tumors. Interestingly, while we found a significant increase in CD34 area in tumors with a high expression of CD93 (Fig. 7B), CD34 area *per se* did not correlate to increased patient survival ($P = 0.5006$, Cox regression model). This indicates that high CD93 expression and alteration of the vascular phenotype are associated with poor survival in these tumors, consistent with the proposed biologic role of CD93 in the tumor vasculature of human gliomas.

Discussion

Extensive angiogenesis and markedly abnormal blood vessels are a hallmark of grade IV glioma and the abnormal, malfunctioning vessels contribute to the severity of the disease. Previously, we reported that these pathologically altered vessels in grade IV glioma express high levels of CD93, a transmembrane protein from the C-type superfamily of lectins with a calcium-dependent carbohydrate-binding domain (7). CD93 was initially suggested to play a role in angiogenesis due to its high expression in areas of blood vessel remodeling in the developing vasculature of mouse embryos (24). We now demonstrate that CD93 has a functional role in modulating angiogenesis and vascular function in glioma, and that high level of CD93 protein correlates with shorter survival in patients with high-grade astrocytic gliomas.

In line with our initial finding on elevated CD93 expression in glioblastoma vasculature, a subsequent study identified CD93 as one of the top genes of a core human primary tumor angiogenesis signature, highly expressed in head and neck squamous cell carcinomas, breast cancers, and clear cell renal cell carcinomas (7, 15). These studies are the first ones to report CD93 as a tumor vascular marker. The other Group XIV members of the C-type lectin superfamily, such as thrombomodulin and endosialin (also known as tumor endothelial marker TEM1), have already in earlier studies been reported to be highly expressed in malignant tumor vasculature, including brain tumors (8, 25–27).

The high level of CD93 expression and its correlation with a poor survival outcome in glioblastoma patients warrant studies aimed at understanding the effect of CD93 on glioma development. To this end, we employed the GL261 mouse glioma model, which is an excellent model for our purpose, as its vascular phenotype and CD93 expression pattern mimic that of human glioblastoma. We showed that the absence of CD93 in female mice leads to delayed outgrowth of GL261 glioma and improved survival. This was associated with a strikingly increased permeability and a reduced perfusion of the glioma vasculature in CD93-deficient mice. Together with our *in vitro* observations that CD93 is essential for the establishment of endothelial cell–cell and cell–matrix contacts, migration, and tubular morphogenesis, these data suggest that CD93 promotes the formation of well-functioning tumor vessels. Our observations furthermore suggest that defects in interendothelial junctions and increased permeability in the absence of CD93, rather than lack of lumen formation, underlie its effect on vascular perfusion. Our data are in line with a recently published study by Orlandini and colleagues that reported that a monoclonal antibody to CD93 is able to inhibit the formation of vessel-like structures by HDMEC on Matrigel *in vitro* and *in vivo*, suggesting that antibody targeting of CD93 may inhibit tumor angiogenesis (17). Similar to our studies, the authors also showed that CD93 silencing by lentiviral-mediated expression of a small hairpin RNA impairs human endothelial cell migration and sprouting *in vitro*. However, although Orlandini and colleagues demonstrated that shRNA-mediated knockdown of CD93 inhibited proliferation of HUVEC, we could not confirm that in our HDMEC. Altogether, these data suggest that CD93 is a potential target for antiangiogenic therapy for cancer.

It is not known whether the extracellular N-terminal domain of CD93 binds to other molecules. Although CD93 was once thought to be the receptor for complement component C1q (10), more recent studies demonstrated that C1q-mediated phagocytosis does not depend on CD93 (13) and that CD93

(*Continued.*) In addition, the reverse experiment was performed. Phalloidin Alexa 647 labeling (depicted in green) was used to visualize the unlabeled cells as well. Only the control-transfected cells contributed to the formation of tube-like structures, whereas cells transfected with siRNA to CD93 did not take part in the tube-forming network. I–P, formation of luminized tube-like structures by HDMEC. HDMEC transfected with siRNA to CD93 and control-transfected cells were allowed to form tube-like structures on a 3D collagen gel under VEGF stimulation for 3 days, fixed and stained with 1% toluidin blue. The lower-magnification pictures (I–L; ×10 objective) show impaired tube-like structure formation upon CD93 knockdown (siCD93_1 and siCD93_5) compared with control cells (Mock and siCtrl). The high-magnification pictures (M–P; ×40 objective) demonstrate that both control and CD93 knockdown cells are able to form luminized tubular structures (arrowheads).

Published OnlineFirst September 11, 2015; DOI: 10.1158/0008-5472.CAN-14-3636

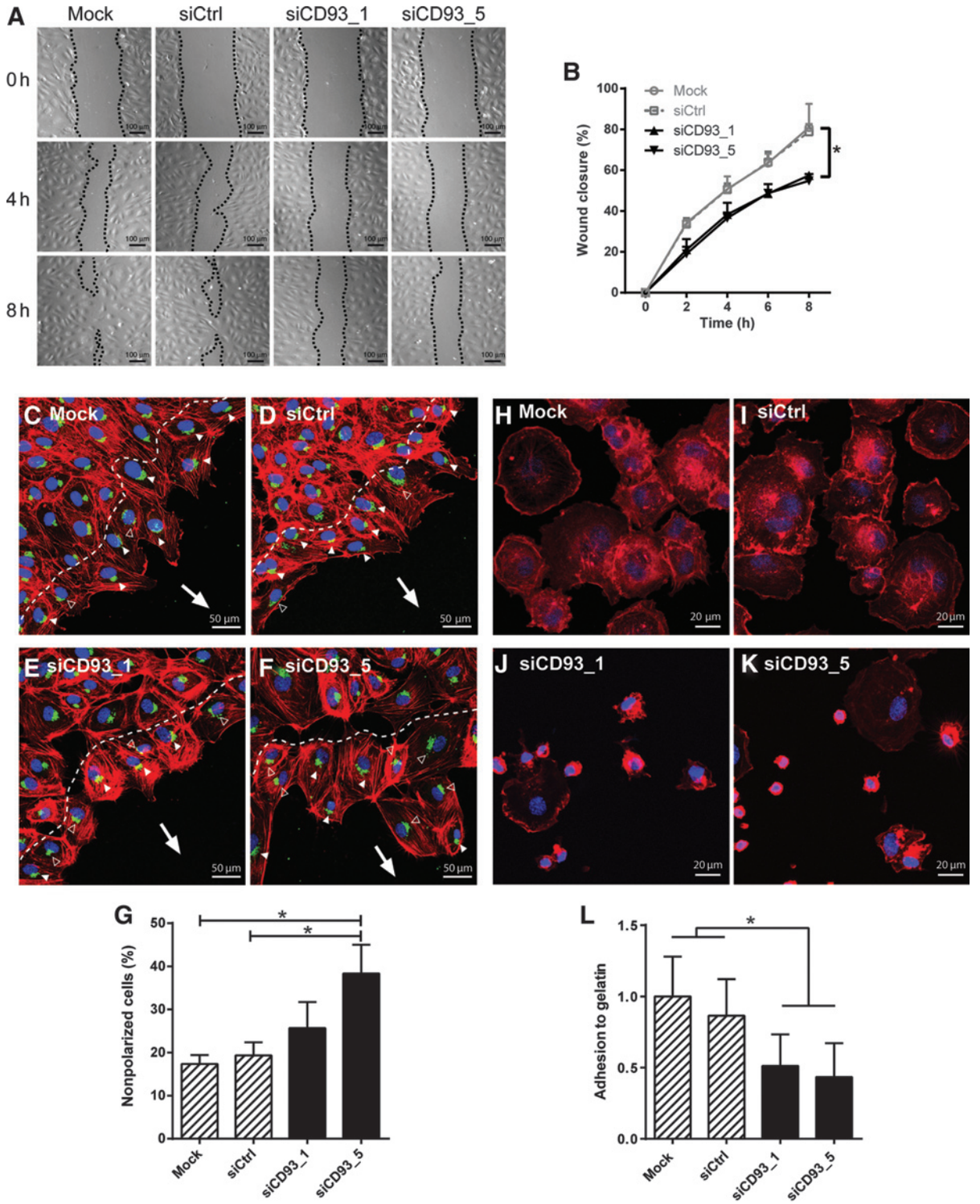

Figure 4.
CD93 knockdown impaired migration, polarization, and cell–matrix adhesion of HDMEC. A and B, migration of HDMEC in a scratch assay. Values represent quantification of wound closure at different time points after the scratch (B; mean + SD of three separate experiments; *, $P < 0.05$, Student *t* test). C–G, immunofluorescent labeling with Golgin-97 (green) and phalloidin (red) of HDMEC in the migrating front of a scratch assay. Large arrows depict the direction of migration. The number of polarized cells (closed arrowheads) and nonpolarized cells (open arrow heads) in the leading edge was counted and the percentage of nonpolarized cells was calculated (G; mean + SD of three separate experiments; *, $P < 0.05$, Student *t* test). H–L, adhesion of HDMEC to gelatin-coated plates at 30 minutes after seeding. Immunofluorescent labeling with phalloidin (red) revealed a difference in cell spreading after CD93 knockdown. Quantification of number of adhering cells (L; mean + SD of three separate experiments, 10 wells per condition; *, $P < 0.05$, one-way ANOVA with Bonferroni correction).

Published OnlineFirst September 11, 2015; DOI: 10.1158/0008-5472.CAN-14-3636

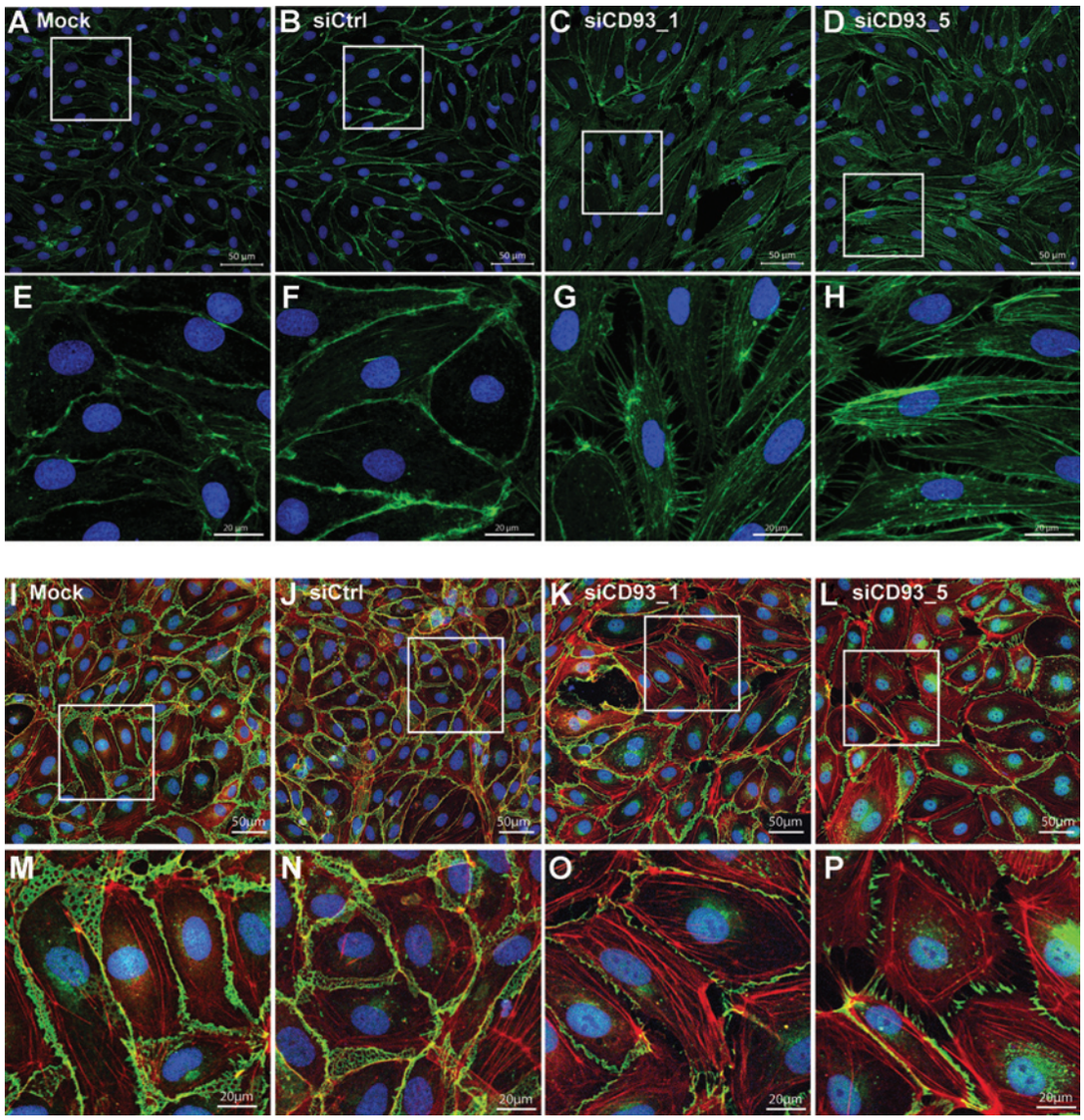

Figure 5.
CD93 knockdown affected cytoskeletal organization and cell–cell junctions in HDMEC. A–H, immunofluorescent labeling of control-transfected HDMEC and HDMEC transfected with siRNA to CD93 with phalloidin to visualize the actin cytoskeleton (green). Enlargements of the insets show an increase in actin stress fiber formation. I–P, immunofluorescent labeling with VE-cadherin (green) and phalloidin (red) of control-transfected HDMEC and HDMEC transfected with siRNA to CD93. The enlarged pictures show a clear inability of siCD93-transfected HDMEC to interact with neighboring cells.

does not bind C1q (28, 29). The intracellular C-terminal domain of CD93 interacts with moesin, a member of the ERM family of proteins that can link CD93 to the cytoskeleton. Such linkage of transmembrane proteins to cytoskeletal actin has been shown to contribute to a redistribution of the actin cytoskeleton that is essential for migration and adhesion (30). This could explain the reduction in cell migration and adhesion, and the abnormal cytoskeletal phenotype in endothelial cells upon CD93 knockdown. Similarly, another Group XIV member of the C-type lectin superfamily, thrombomodulin, controls morphology and migration of epithelial cells via the ERM protein ezrin (31). The linkage of CD93 to the actin cytoskeleton is also essential for its previously described role in phagocytosis (22, 32). Previous studies have pointed to a role for CD93 in leukocyte infiltration in various inflammatory models (33, 34). However, we did not detect any difference in leukocyte infiltration into GL261 and T241 tumors between CD93-deficient and wild-type mice (Supplementary Fig. S4D and S4E). This suggests that CD93-expressing leukocytes do not affect GL261 progression, consistent with CD93 being expressed exclusively by tumor vessels in this model.

An interesting observation is that the absence of CD93 delayed tumor growth only in female mice, both in GL261 gliomas and T241 fibrosarcomas. As CD93 is mainly vascular-expressed, this points to a sex difference either in the vasculature or in tumor growth in these mouse models. Sex hormones have been demonstrated to affect endothelial cell biology, angiogenesis, blood vessel function, and the incidence and pathology of cardiovascular diseases (35–37). Moreover, cancer

Published OnlineFirst September 11, 2015; DOI: 10.1158/0008-5472.CAN-14-3636

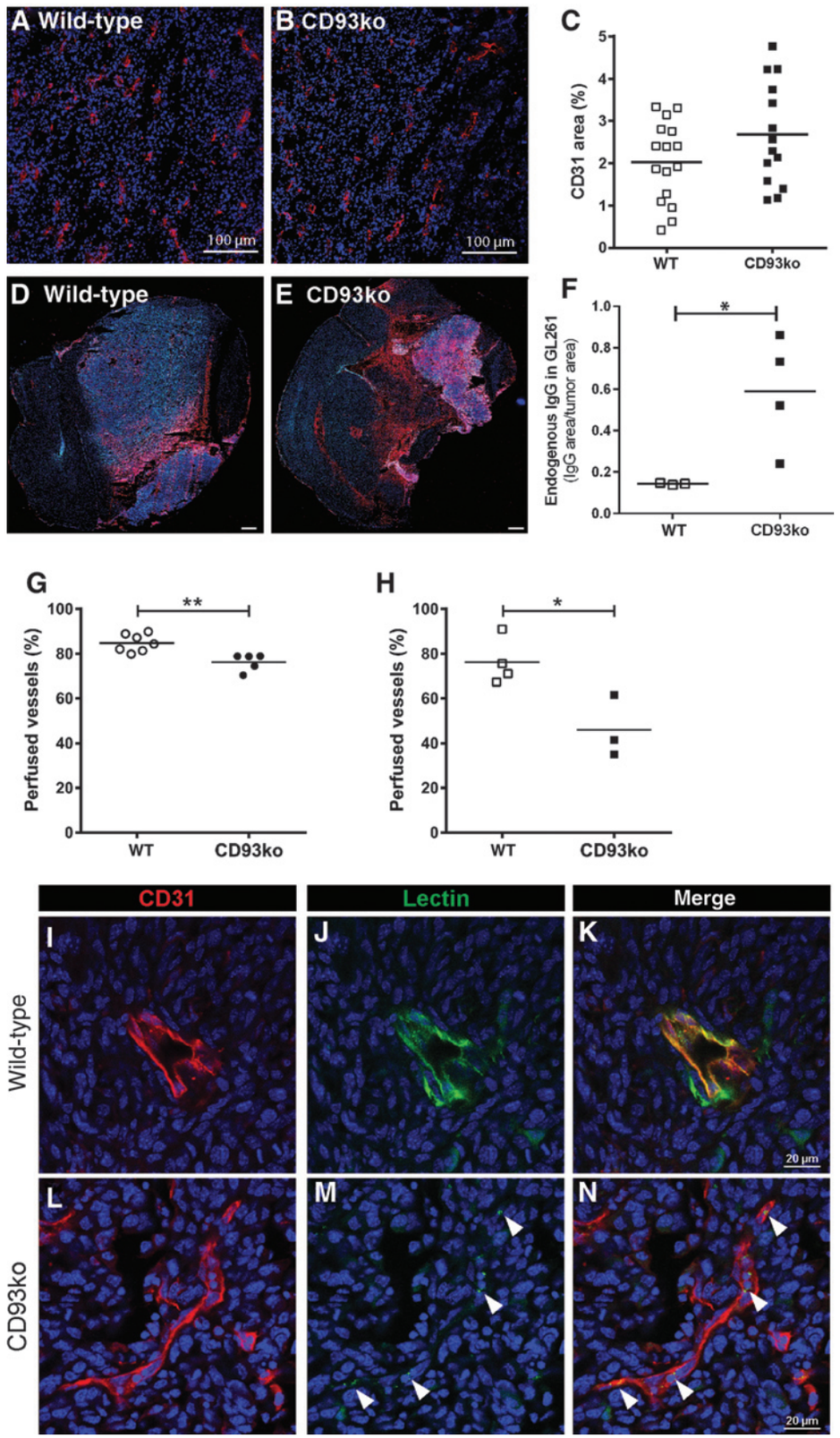

Figure 6.
CD93 deficiency impaired vascular perfusion in GL261 glioma. A and B, immunofluorescent staining of GL261 glioma for CD31 revealed no gross difference in vessel morphology, images taken at ×10 magnification. C, quantification of CD31-positive vascular surface area in GL261 glioma (mean, $n = 14$–16, Mann–Whitney U test and Student t test revealed no statistically significant difference). D and E, immunofluorescent staining of GL261 glioma for endogenous IgG revealed increased tumor vascular permeability in CD93$^{-/-}$ mice compared with wild-type (wt) mice. Scale bar, 500 μm. F, quantification of endogenous IgG relative to total tumor area in wild-type and CD93$^{-/-}$ mice (mean, $n = 3$–4, Student t test). G–N, GL261 glioma-bearing male (G) and female (H) mice were perfused with respectively FITC-labeled or biotin-labeled lycopersicon esculentum (tomato) lectin. Brain tumor cryosections or vibratome sections were immunofluorescently stained for CD31 to visualize the vasculature, and the number of perfused vessels was quantified and expressed as a percentage of total vessel number (G and H; $n = 3$–7, 5 representative images were analyzed per mouse; *, $P < 0.05$; **, $P < 0.01$, Student t test). Blood vessels were considered perfused even when small traces of lectin were visible. The blood vessel of the CD93$^{-/-}$ mouse in the graph is therefore counted as positive in the quantification (I–N). Yet, the presence of FITC-lectin was limited to only certain spots in the majority of perfused vessels in CD93$^{-/-}$ mice, whereas FITC-lectin perfusion covered the whole vascular lining in blood vessels of wild-type mice.

Published OnlineFirst September 11, 2015; DOI: 10.1158/0008-5472.CAN-14-3636

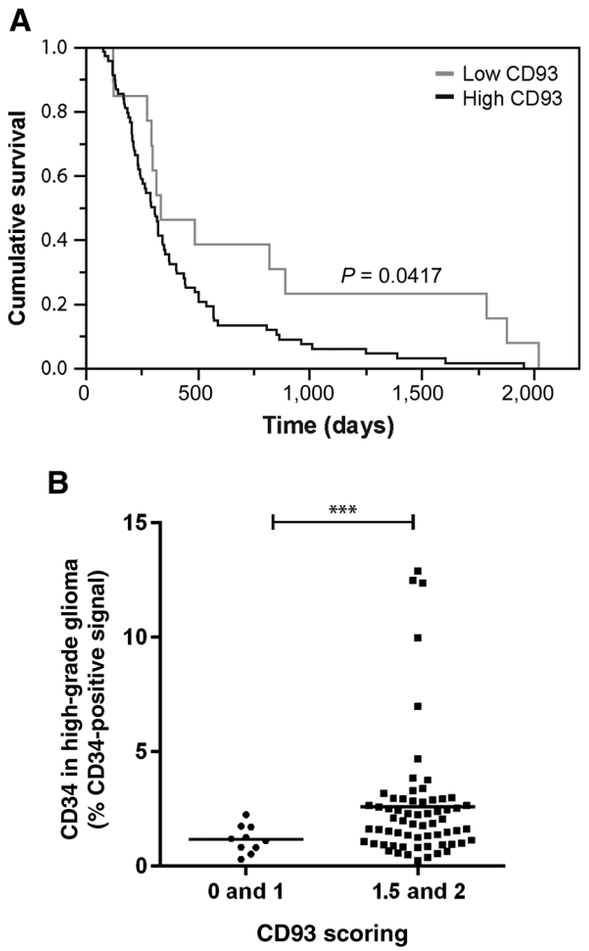

Figure 7.
High vascular CD93 expression in human glioma correlated with poor survival. A, Kaplan–Meier curves of high-grade glioma patients (grades III and IV) with low vascular CD93 expression (average CD93 score of 0 or 1, $n = 13$) or high vascular CD93 expression (average CD93 score of 1.5 or 2, $n = 68$). Statistical analysis of survival rates was assessed by univariate (log-rank test, $P = 0.0471$) and multivariate (Cox proportional hazards, $P = 0.0479$) models. B, correlation between vascularity and CD93 expression in high-grade glioma (grade III and grade IV). The graph represents the percentage of the CD34-positive area compared with CD93 expression scoring (CD93 score, 0–1 and 1.5–2; $n = 29, 108$; ***, $P < 0.001$, Mann–Whitney *U* test and Student *t* test).

susceptibility is different between the two sexes for many types of cancer (38), and glioblastomas are 40% more common in men than in women (1, 39). Of note, however, is the observation that even though the absence of CD93 did not affect tumor growth speed in male mice, it impaired perfusion of the glioma vasculature in male mice equally well as in female mice. This suggests that CD93 controls vascular function both in males and females. Among human glioma patients, CD93 was expressed to an equal extent in tumor vessels of men and women, and the correlation to poor survival was only significant when both men and women were included in the survival analysis (Supplementary Fig. S6A–S6D).

Taken together, our data imply that CD93 is a key regulator of glioma angiogenesis. Through the control of cell–cell and cell–matrix adhesion, CD93 controls vessel architecture during pathologic angiogenesis and promotes tumor progression by enhancing the formation of well-functioning tumor vessels. As the CD93 expression level correlates with survival of patients with high-grade astrocytic gliomas, future studies should focus on evaluating its potential as therapeutic target for antiangiogenic therapy or as a biomarker for glioblastoma progression.

Disclosure of Potential Conflicts of Interest

No potential conflicts of interest were disclosed.

Authors' Contributions

Conception and design: E. Langenkamp, R. Lugano, A. Dimberg
Development of methodology: E. Langenkamp, L. Zhang, M. Essand
Acquisition of data (provided animals, acquired and managed patients, provided facilities, etc.): E. Langenkamp, L. Zhang, R. Lugano, H. Huang, M. Georganaki, W. Bazzar, J. Lööf, G. Trendelenburg, F. Pontén, A. Smits, A. Dimberg
Analysis and interpretation of data (e.g., statistical analysis, biostatistics, computational analysis): E. Langenkamp, R. Lugano, T.E.A. Elhassan, M. Georganaki, W. Bazzar, J. Lööf, A. Smits, A. Dimberg
Writing, review, and/or revision of the manuscript: E. Langenkamp, R. Lugano, T.E.A. Elhassan, G. Trendelenburg, A. Smits, A. Dimberg
Administrative, technical, or material support (i.e., reporting or organizing data, constructing databases): E. Langenkamp, H. Huang, F. Pontén
Study supervision: A. Dimberg

Acknowledgments

The authors thank Dr. Michael Bergqvist and Dr. Simon Ekman, Department of Radiology, Oncology and Radiation Science, Uppsala University, for access to tissue microarrays of high-grade glioma patients. Imaging was performed with equipment maintained by the Science for Life Lab BioVis Platform, Uppsala.

Grant Support

This work was supported by grants from the Swedish Cancer Society (CAN 2011/862), the Swedish Childhood Cancer Society (PR2013-0107, PROJ11/083), and the Swedish Research Council (2013–3797, 2008–2853).

The costs of publication of this article were defrayed in part by the payment of page charges. This article must therefore be hereby marked *advertisement* in accordance with 18 U.S.C. Section 1734 solely to indicate this fact.

Received December 17, 2014; revised July 17, 2015; accepted July 26, 2015; published OnlineFirst September 11, 2015.

References

1. Wen PY, Kesari S. Malignant gliomas in adults. N Engl J Med 2008; 359:492–507.
2. Louis DN, Ohgaki H, Wiestler OD, Cavenee WK, Burger PC, Jouvet A, et al. The 2007 WHO classification of tumours of the central nervous system. Acta Neuropathol 2007;114:97–109.
3. Jain RK, di Tomaso E, Duda DG, Loeffler JS, Sorensen AG, Batchelor TT. Angiogenesis in brain tumours. Nat Rev Neurosci 2007;8:610–22.
4. Jansen M, de Witt Hamer PC, Witmer AN, Troost D, van Noorden CJ. Current perspectives on antiangiogenesis strategies in the treatment of malignant gliomas. Brain Res Brain Res Rev 2004;45:143–63.

Published OnlineFirst September 11, 2015; DOI: 10.1158/0008-5472.CAN-14-3636

5. Wong ML, Prawira A, Kaye AH, Hovens CM. Tumour angiogenesis: its mechanism and therapeutic implications in malignant gliomas. J Clin Neurosci 2009;16:1119–30.
6. Langenkamp E, Molema G. Microvascular endothelial cell heterogeneity: general concepts and pharmacological consequences for anti-angiogenic therapy of cancer. Cell Tissue Res 2009;335:205–22.
7. Dieterich LC, Mellberg S, Langenkamp E, Zhang L, Zieba A, Salomaki H, et al. Transcriptional profiling of human glioblastoma vessels indicates a key role of VEGF-A and TGF-beta2 in vascular abnormalization. J Pathol 2012;228:378–90.
8. St. Croix B, Rago C, Velculescu V, Traverso G, Romans KE, Montgomery E, et al. Genes expressed in human tumor endothelium. Science 2000;289: 1197–202.
9. Langenkamp E, Vom Hagen FM, Zwiers PJ, Moorlag HE, Schouten JP, Hammes HP, et al. Tumor vascular morphology undergoes dramatic changes during outgrowth of B16 melanoma while proangiogenic gene expression remains unchanged. ISRN Oncol 2011;2011:409308.
10. Nepomuceno RR, Henschen-Edman AH, Burgess WH, Tenner AJ. cDNA cloning and primary structure analysis of C1qR(P), the human C1q/MBL/SPA receptor that mediates enhanced phagocytosis in vitro. Immunity 1997;6:119–29.
11. Bohlson SS, Silva R, Fonseca MI, Tenner AJ. CD93 is rapidly shed from the surface of human myeloid cells and the soluble form is detected in human plasma. J Immunol 2005;175:1239–47.
12. Greenlee MC, Sullivan SA, Bohlson SS. Detection and characterization of soluble CD93 released during inflammation. Inflamm Res 2009;58: 909–19.
13. Norsworthy PJ, Fossati-Jimack L, Cortes-Hernandez J, Taylor PR, Bygrave AE, Thompson RD, et al. Murine CD93 (C1qRp) contributes to the removal of apoptotic cells in vivo but is not required for C1q-mediated enhancement of phagocytosis. J Immunol 2004;172:3406–14.
14. Chevrier S, Genton C, Kallies A, Karnowski A, Otten LA, Malissen B, et al. CD93 is required for maintenance of antibody secretion and persistence of plasma cells in the bone marrow niche. Proc Natl Acad Sci U S A 2009;106:3895–900.
15. Masiero M, Simoes FC, Han HD, Snell C, Peterkin T, Bridges E, et al. A core human primary tumor angiogenesis signature identifies the endothelial orphan receptor ELTD1 as a key regulator of angiogenesis. Cancer Cell 2013;24:229–41.
16. Kao YC, Jiang SJ, Pan WA, Wang KC, Chen PK, Wei HJ, et al. The epidermal growth factor-like domain of CD93 is a potent angiogenic factor. PloS One 2012;7:e51647.
17. Orlandini M, Galvagni F, Bardelli M, Rocchigiani M, Lentucci C, Anselmi F, et al. The characterization of a novel monoclonal antibody against CD93 unveils a new antiangiogenic target. Oncotarget 2014;5:2750–60.
18. Uhlen M, Oksvold P, Fagerberg L, Lundberg E, Jonasson K, Forsberg M, et al. Towards a knowledge-based Human Protein Atlas. Nat Biotechnol 2010;28:1248–50.
19. Mellberg S, Dimberg A, Bahram F, Hayashi M, Rennel E, Ameur A, et al. Transcriptional profiling reveals a critical role for tyrosine phosphatase VE-PTP in regulation of VEGFR2 activity and endothelial cell morphogenesis. FASEB J 2009;23:1490–502.
20. Koh W, Stratman AN, Sacharidou A, Davis GE. In vitro three dimensional collagen matrix models of endothelial lumen formation during vasculogenesis and angiogenesis. Methods Enzymol 2008;443: 83–101.
21. Bisel B, Calamai M, Vanzi F, Pavone FS. Decoupling polarization of the Golgi apparatus and GM1 in the plasma membrane. PLoS One 2013;8: e80446.
22. Zhang M, Bohlson SS, Dy M, Tenner AJ. Modulated interaction of the ERM protein, moesin, with CD93. Immunology. 2005;115:63–73.
23. Elsir T, Edqvist PH, Carlson J, Ribom D, Bergqvist M, Ekman S, et al. A study of embryonic stem cell-related proteins in human astrocytomas: identification of Nanog as a predictor of survival. Int J Cancer 2014; 134:1123–31.
24. Petrenko O, Beavis A, Klaine M, Kittappa R, Godin I, Lemischka IR. The molecular characterization of the fetal stem cell marker AA4. Immunity 1999;10:691–700.
25. Maruno M, Yoshimine T, Isaka T, Kuroda R, Ishii H, Hayakawa T. Expression of thrombomodulin in astrocytomas of various malignancy and in gliotic and normal brains. J Neurooncol 1994;19:155–60.
26. Carson-Walter EB, Winans BN, Whiteman MC, Liu Y, Jarvela S, Haapasalo H, et al. Characterization of TEM1/endosialin in human and murine brain tumors. BMC Cancer 2009;9:417.
27. Maia M, DeVriese A, Janssens T, Moons M, Lories RJ, Tavernier J, et al. CD248 facilitates tumor growth via its cytoplasmic domain. BMC Cancer 2011;11:162.
28. McGreal EP, Ikewaki N, Akatsu H, Morgan BP, Gasque P. Human C1qRp is identical with CD93 and the mNI-11 antigen but does not bind C1q. J Immunol 2002;168:5222–32.
29. Greenlee-Wacker MC, Galvan MD, Bohlson SS. CD93: recent advances and implications in disease. Curr Drug Targets 2012;13:411–20.
30. Tsukita S, Yonemura S. Cortical actin organization: lessons from ERM (ezrin/radixin/moesin) proteins. J Biol Chem 1999;274:34507–10.
31. Hsu YY, Shi GY, Kuo CH, Liu SL, Wu CM, Ma CY, et al. Thrombomodulin is an ezrin-interacting protein that controls epithelial morphology and promotes collective cell migration. Faseb J 2012;26:3440–52.
32. Greenlee MC, Sullivan SA, Bohlson SS. CD93 and related family members: their role in innate immunity. Curr Drug Targets 2008;9:130–8.
33. Harhausen D, Prinz V, Ziegler G, Gertz K, Endres M, Lehrach H, et al. CD93/AA4.1: a novel regulator of inflammation in murine focal cerebral ischemia. J Immunol 2010;184:6407–17.
34. Greenlee-Wacker MC, Briseno C, Galvan M, Moriel G, Velazquez P, Bohlson SS. Membrane-associated CD93 regulates leukocyte migration and C1q-hemolytic activity during murine peritonitis. J Immunol 2011; 187:3353–61.
35. Sieveking DP, Lim P, Chow RW, Dunn LL, Bao S, McGrath KC, et al. A sex-specific role for androgens in angiogenesis. J Exp Med 2010;207: 345–52.
36. Sader MA, Celermajer DS. Endothelial function, vascular reactivity and gender differences in the cardiovascular system. Cardiovasc Res 2002;53: 597–604.
37. Pepine CJ, Nichols WW, Pauly DF. Estrogen and different aspects of vascular disease in women and men. Circ Res 2006;99:459–61.
38. Dorak MT, Karpuzoglu E. Gender differences in cancer susceptibility: an inadequately addressed issue. Front Genet 2012;3:268.
39. Ricard D, Idbaih A, Ducray F, Lahutte M, Hoang-Xuan K, Delattre JY. Primary brain tumours in adults. Lancet 2012;379:1984–96.

Published OnlineFirst September 11, 2015; DOI: 10.1158/0008-5472.CAN-14-3636

Cancer Research
The Journal of Cancer Research (1916–1930) | The American Journal of Cancer (1931–1940)

AACR American Association for Cancer Research

Elevated Expression of the C-Type Lectin CD93 in the Glioblastoma Vasculature Regulates Cytoskeletal Rearrangements That Enhance Vessel Function and Reduce Host Survival

Elise Langenkamp, Lei Zhang, Roberta Lugano, et al.

Cancer Res 2015;75:4504-4516. Published OnlineFirst September 11, 2015.